Pharmaceutical Research, Vol. 25, No. 11, November 2008 (© 2008)
DOI: 10.1007/s11095-008-9659-3

Research Paper

Flocculated Amorphous Nanoparticles for Highly Supersaturated Solutions

Michal E. Matteucci,[1] Joseph C. Paguio,[1] Maria A. Miller,[1] Robert O. Williams III,[2] and Keith P. Johnston[1,3]

Received March 21, 2008; accepted June 9, 2008; published online August 15, 2008

Purpose. To recover polymer-stabilized amorphous nanoparticles from aqueous dispersions efficiently by salt flocculation and to show that the particles redisperse and dissolve rapidly to produce highly supersaturated solutions.
Methods. Nanoparticle dispersions of itraconazole stabilized by nonionic polymers were formed by antisolvent precipitation and immediately flocculated with sodium sulfate, filtered and dried. The size after redispersion in water, crystallinity, and morphology were compared with those for particles produced by spray drying and rapid freezing.
Results. Particle drug loading increased to ~90% after salt flocculation and removal of excess polymer with the filtrate. The formation of the flocs at constant particle volume fraction led to low fractal dimensions (open flocs), which facilitated redispersion in water to the original primary particle size of ~300 nm. Amorphous particles, which were preserved throughout the flocculation–filtration–drying process, dissolved to supersaturation levels of up to 14 in pH 6.8 media. In contrast, both spray dried and rapidly frozen nanoparticle dispersions crystallized and did not produce submicron particle dispersions upon addition to water, nor high supersaturation values.
Conclusions. Salt flocculation produces large yields of high surface area amorphous nanoparticle powders that de-aggregate and dissolve rapidly upon redispersion in pH 6.8 media, for supersaturation levels up to 14.

KEY WORDS: amorphous drug; nanoparticle filtration; nanoparticle recovery; salt flocculation; supersaturation.

INTRODUCTION

For a large fraction of newly discovered drugs, bioavailability is limited by poor solubility in water (1). Amorphous nanoparticles with high surface area may be designed to raise dissolution rates as well as to achieve high levels of supersaturation. An increase in supersaturation in the gastrointestinal tract would lead to greater flux through biomembranes (2,3) and higher bioavailability. Solubilities of amorphous drugs may reach 1,600-times that of the crystalline form (4–7). Typically, amorphous solid solutions or dispersions of drugs, stabilized by high glass transition (T_g) polymers, are formulated by co-grinding (8), solvent evaporation (9–13), or hot melt extrusion (14,15). Amorphous formulations, however, have a tendency to crystallize during dissolution (16). This crystallization may be minimized by designing rapidly dissolving nanoparticles, with surface areas on the order of 50 m^2/g, particularly for slowly dissolving stabilizers such as hydroxypropylmethylcellulose (7). High surface area amorphous micro- (16,17) and nanoparticles (18,19) may be formed by rapid nucleation from solution along with arrested growth. For example, in antisolvent precipitation of organic solutions mixed with aqueous media, preferential adsorption of the stabilizer at the particle surface inhibits nanoparticle growth and crystallization even with drug loadings of 94% (drug wt./tot. wt.) (7).

A wide variety of techniques have been developed to form inorganic and pharmaceutical nanocrystals in the presence of stabilizers, such as mechanical milling (20–22), physical changes in solvent properties like antisolvent precipitation (18,23–26), and by chemical reactions, for example thermal decomposition (27). However, the recovery of the nanoparticles from solution and further processing of the nanocrystals in the solid state remains a formidable challenge. Common techniques for solvent removal include spray drying, freeze drying and ultrafiltration. Spray drying is energy intensive and yields can be limited. The elevated temperatures of 90°C or higher, and an increase in volume fraction of the particles during droplet shrinkage, may cause crystallization or particle growth by the increase in the collision rates and/or Ostwald ripening. In addition, loss in solvent quality at elevated temperatures may lead to collapse of polymeric steric stabilizers (28–30). Tray lyophilization requires extremely long processing times. During freezing processes, particles are concentrated in the unfrozen aqueous phase as ice crystals are removed. Again the increase in particle concentration and changes in solvent quality may

[1] Department of Chemical Engineering, The University of Texas at Austin, 1 University Station CO400, Austin, Texas 78712, USA.
[2] College of Pharmacy, University of Texas at Austin, Austin, Texas 78712, USA.
[3] To whom correspondence should be addressed. (e-mail: kpj@che.utexas.edu)

cause particle crystallization and growth. Ultrafiltration of nanoparticles has also been used to purify nanoparticle dispersions (31); however, filtrate removal rates were limited to ~0.03 ml/min cm^2, even for a membrane surface area of 1,000 cm^2, and the dispersion could only be concentrated by a factor of 1/5. Long filtration times allow for particle growth via Ostwald ripening and coagulation. It would be desirable to develop novel rapid techniques for particle recovery and solvent removal to avoid undesired crystallization and growth and to increase production rates of dry powders in a useful morphology for subsequent processing.

An alternative approach is to flocculate nanoparticles reversibly to form large flocs that may be filtered rapidly (32, 33). Flocculation of negatively charged gold nanoparticles with positively charged poly(L-lysine) created spherical submicron aggregates, which formed unique 1–5 μm hollow spheres upon subsequent addition of SiO_2 nanoparticles (34). Flocculation may also be produced by adding electrolytes to weaken the hydration of the stabilizers on the nanocrystal surface, resulting in interparticle attractive interactions. Electrolytes decrease the lower critical solution temperature (LCST) of poly(ethyleneoxide) (PEO) chains (35–39) by inducing desolvation of the ether oxygens. The LCST corresponds to the critical flocculation temperature (CFT) of the particle dispersion for micron sized particles stabilized by PEO containing copolymers (29,40,41). A recent study has utilized Na_2SO_4 to flocculate crystalline naproxen nanoparticles stabilized by poly(vinylpyrrolidone) or PEO chains (32,33). Aqueous suspensions (50 ml) of the large flocs were filtered in minutes to obtain a dry powder. The dried powders were redispersible to the original 300 nm particle size and drug yields after filtration were as high as 99% (wt. recovered drug/ wt. input drug). Alternatively, addition of Na_2SO_4 or KCl to sterically stabilized platinum catalyst nanoparticles induced instability as evident by turbidimetry (42). However, these nanoparticles were not filtered or shown to redisperse to the original size.

The objectives of the current study were to produce flocs of amorphous polymer-stabilized nanoparticles, which may be filtered, dried, and redispersed, to achieve (1) the original primary particle sizes and (2) rapid generation of supersaturated solutions up to 14-times the crystalline solubility, despite drug loadings up to 94%. This study extends our previous work (32,33) on flocculation of nanoparticle crystalline drugs to include amorphous morphologies. In addition, we compare the mechanisms of particle aggregation and redispersion for salt flocculation relative to spray drying and rapid freezing as a function of changes in particle volume fraction ϕ and solvent quality for the stabilizers. Whereas ϕ increases in spray drying and rapid freezing during water removal, it remains constant during salt flocculation. The differences in the pathways in particle volume fraction and solvent conditions, as a function of temperature and salinity, will be shown to have a profound effect on the particle size upon redispersion and level of supersaturation as the particles dissolve. The rapid change of interparticle forces from repulsive to attractive, upon addition of salt, produces open flocs with low fractal dimensions. Consequently, the flocs redisperse rapidly to the original primary particle size in water. The size of the redispersed particles will be shown to be much smaller than for the more compact flocs produced by freezing/lyophilization. Additionally, low temperatures and rapid removal of solvent during filtration will be utilized to preserve the amorphous morphology of the nanoparticles more effectively than in the case of spray drying, as demonstrated by modulated differential scanning calorimetry and by high supersaturation levels in pH 6.8 media. The rapid dissolution of nanoparticles recovered by salt flocculation will be shown to prevent significant crystallization of the undissolved solid phase during dissolution, leading to high supersaturation values, with the potential to enhance bioavailability.

EXPERIMENTAL

Materials

B.P. grade itraconazole (Itz) was purchased from Hawkins, Inc. (Minneapolis, MN). Hydroxypropylmethylcellulose E5 grade (HPMC) (viscosity of 5 cP at 2% aqueous 25°C solution) was a gift from The Dow Chemical Corporation. Poly(ethylene oxide-*b*-propylene oxide-*b*-ethylene oxide) (P407) with a nominal molecular weight of 12,500 and a PEO/PPO ratio of 2:1 by weight was purchased from Spectrum Chemical Manufacturing Corporation (Gardena, CA). Stabilized p.a. grade 1,3-dioxolane was obtained from Acros Organics (Morris Plains, NJ). HPLC grade acetonitrile (ACN), A.C.S. grade hydrochloric acid (HCl), diethanolamine (DEA), sodium dodecyl sulfate (SDS), and sodium sulfate anhydrous (Na_2SO_4) were used as received from Fisher Chemicals (Fairlawn, NJ). A glass transition temperature (T_g) of 154°C has been reported for HPMC E5 (43) and estimated as −21°C for P407. Type P2 filter paper with an area of 95 cm^2 and an estimated pore size of 1–3 μm was purchased from Fisher Scientific (Atlanta, GA).

Precipitation of Itz Nanoparticles into Aqueous Solution

Using an antisolvent precipitation method (18), nanoparticle dispersions of Itz were produced at ~3°C. Deionized water (50 ml) containing an appropriate quantity of HPMC was used as the antisolvent phase into which 15 g of 1,3-dioxolane containing 3.3% (wt) Itz (and P407 in some cases) was injected using a 19 G needle in approximately 6 s to form a fine precipitate. A control experiment was performed in which the nanocrystals were recovered by rapid freezing and lyophilization. For this rapidly frozen control, the organic phase was first separated from the aqueous dispersion via vacuum distillation at 40 Torr and 38°C. The aqueous dispersion was added dropwise to liquid nitrogen and lyophilized to form a powder using a Virtis Advantage Tray Lyophilizer (Virtis Company, Gardiner, NY) with 24 h of primary drying at −35°C followed by 36 h of secondary drying at 25°C. Unless noted otherwise, the particle size distributions of the original dispersion and the redispersed flocs were determined by static light scattering using a Malvern Mastersizer-S (Malvern Instruments Ltd., UK).

Spray Drying of Itz Nanoparticle Dispersions

After vacuum distillation the aqueous dispersion was spray dried using a Buchi mini-spray dryer Model 190 (Brinkmann Instruments Co., Westbury, New York) equipped

with a 0.7 mm diameter two-fluid nozzle. Compressed air at 120 psi was used for the atomizing nozzle, with the flow rate controlled to 200 ml/s. The dispersion was fed at a rate of 5 ml/min. An inlet temperature of 140°C and outlet temperature of 90°C were maintained throughout the process.

Heating of Itz Nanoparticle Dispersions

Dispersions were heated after organic solvent removal either rapidly to 98°C, or slowly to 92°C. For rapid heating, the dispersion was injected at 10 ml/min through ~3′ of 0.03″ ID stainless steel tubing which was heated by a 98°C water bath. Upon exiting the heat exchanger, the dispersion was immediately quench-cooled into water (3°C). For slow heating, the dispersion was placed in a beaker which was heated at a rate of 2.5°C/min. The dispersion was allowed to remain at 92°C for 10 min before quench cooling in an ice bath. In both cases, particle size measurement was taken immediately after quench cooling using dynamic light scattering.

Flocculation and Rapid Filtration of Itz Nanoparticle Dispersions

After particle size determination, the nanoparticle dispersions were flocculated by addition of a 1.5 M solution of Na_2SO_4 at a volume ratio of 12:5 (salt solution/suspension). This approach produced a SO_4^{-2} concentration of 1 M in the final mixture. Immediately after salt addition, the flocs took up the entire aqueous volume, as seen in Fig. 1B. The flocculated suspension was stored at room temperature for 3 min during which larger flocs formed. The flocs were filtered with 11 cm diameter P2 filter paper (Fisher Scientific, Fair lawn, NJ) under vacuum. The filtration was continued until no water could be observed on top of the filter cake, typically after <8 min. A 30 ml aliquot of HPMC aqueous solution (identical to the antisolvent phase of the sample) was chilled in an ice bath and used to rinse the filter cake immediately after filtration. The filter cake was then allowed to dry at room temperature and atmospheric pressure overnight. Dried powders were obtained by gently scraping the filter paper.

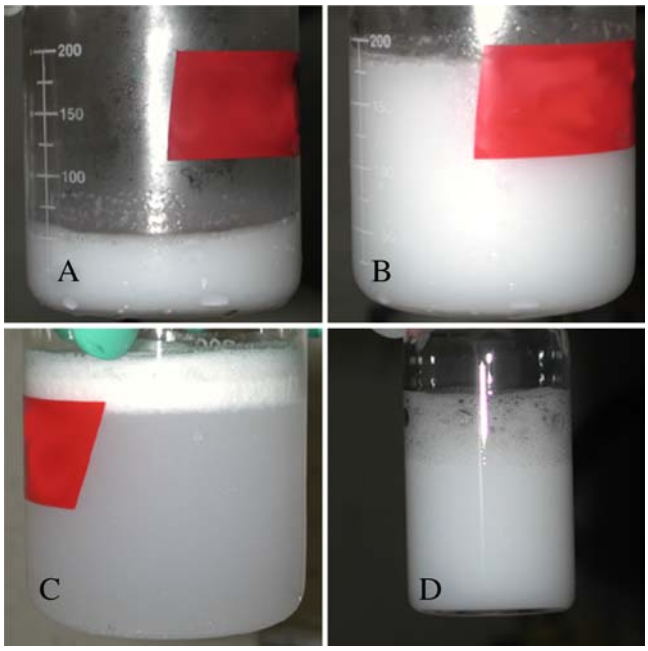

Fig. 1. Progression of salt flocculation: **A** original dispersion; **B** 3 s after salt solution addition; **C** 3 min after salt solution addition; **D** after dry powder redispersion in pure water at ~10 mg/ml.

High Performance Liquid Chromatography (HPLC)

Solutions from dissolution studies and dissolved dried powders were analyzed for drug concentration using a Shimadzu LC-10 liquid chromatograph (Shimadzu Corporation, Columbia, MD) with an Alltech 5 μm Inertsil ODS-2 C18 reverse-phase column (Alltech Aassociates, Inc., Deerfield, IL). The mobile phase was ACN/water/DEA 70:30:0.05 (volume ratio) and the flow rate was 1 ml/min. Using a detection wavelength of 263 nm, the Itz peak eluted at 5.4 min. The standard curve linearity was verified from 500 to 1 μg/ml with an r^2 value of at least 0.999.

Salt and Drug Content Determination

In order to determine the quantity of residual salt in the final filter cake, approximately 15 mg of dried powder was dissolved in 100 ml of 50:50 ACN/water. Using a YSI 3100 conductivity instrument (YSI Inc., Yellow Springs, OH), the conductivity of the solution was determined and compared to a standard curve of Na_2SO_4 for concentrations from 0.004 to 0.137 mg/ml. The standard curve was linear with an r^2 value of 0.9998. The drug concentration of the solution was determined by HPLC and used to calculate the drug loading of the final powder.

Contact Angle

Approximately 50 mg of dried powder was compacted with ~500 kg using a Model M Carver Laboratory Press (Fred S. Carver, Inc., Menomeonee Falls, WI) to form a flat sided pellet. A 10 μl drop of pH 6.8 phosphate buffer without SDS was placed on the pellet, and the contact angle was measured within 15 s using a Model 100-00-115 Goniometer (Rame-Hart Inc., Mountain Lakes, NJ). Measurements were made in quadruplicate and the average and standard deviation were reported, since any cracks or impurities on the flat surface will result in a deviation of the contact angle.

Scanning Electron Microscopy (SEM)

Dried powders were redispersed in pure water at a concentration of approximately 4 mg/ml. Using a Branson Sonifier 250 (VWR Scientific, West Chester, PA), the dispersion was sonicated for 2 min at 50% duty cycle. The aqueous dispersions were then flash frozen onto aluminum SEM stages maintained at −200°C with liquid nitrogen. After lyophilization to remove the water, the remaining particles were gold-palladium sputter coated for 1 min prior to analysis on a Hitachi S-4500 field emission scanning electron microscope at an accelerating voltage of 15 kV.

Temperature Modulated Differential Scanning Calorimetry (mDSC)

Drug powders were placed in hermetically sealed aluminum pans and scanned using a 2920 modulated DSC (TA Instruments, New Castle, DE) with a refrigerated cooling system. The samples were purged with nitrogen at a flow rate of 150 ml/min. The amplitude used was 1°C, the period 1 min, and the underlying heating rate 5°C/min. Both forward and reverse heat flow were used to characterize the thermal transitions of samples.

Dissolution Under Supersaturated Conditions

Solubilities of metastable solutions of amorphous drug and rates of supersaturation were measured in pH 6.8 phosphate buffer made by mixing one part 0.1 N HCl with three parts 0.2 M tribasic sodium phosphate at 37.2°C. In the media with 0.17% (*w*/*v*) SDS, the equilibrium crystalline solubility was 14 μg/ml, as measured in triplicate similarly to the method described in a previous study (7). A USP paddle method was adapted to accommodate the small sample sizes using a VanKel VK6010 Dissolution Tester with a Vanderkamp VK650A heater/circulator (VanKel, Cary, NC) (7). Dissolution media (50 ml) was preheated in small 100 ml capacity dissolution vessels (Varian Inc., Cary, NC). A sample weight (~17.5 mg drug) equivalent to approximately 25-times the equilibrium solubility of Itz in pH 6.8 media containing SDS was added. Sample aliquots (1.5 ml) were taken at various time points. The aliquots were filtered immediately using a 0.2 μm syringe filter and 0.8 ml of the filtrate was subsequently diluted with 0.8 ml of ACN. In all cases, the filtrate was completely clear upon visual inspection and dynamic light scattering of the filtrate gave a count rate of less than 20 kcps (too small for particle size analysis). For all samples, the drug concentration was quantified by HPLC. The supersaturation levels are reported as the drug concentration divided by the crystalline solubility. Supersaturation was plotted *versus* time and the area under the curve (AUC) was calculated using the numerical integration.

RESULTS

Polymer-salt Cloud Points, Particle Properties, and Recovery After Flocculation

The cloud point temperatures of P407 and HPMC over a range of Na_2SO_4 solutions have been reported (33,35,44). On the basis of extrapolation down to 25°C, molarities of approximately 0.55 and 0.8 are needed to precipitate a 2% solution of pure P407 and HPMC, respectively. For the present study, concentrations of HPMC ranged from 0.25% to 1% (*w*/*v*) (formulations A–C, Table I) and P407 concentrations from 0.03% to 0.87% (formulations D–I, Table II). As shown in Table I, a minimum molarity of 0.25 M (after addition of salt solution) was required at 25°C to flocculate particles stabilized by HPMC. In order to ensure complete and rapid flocculation of nanoparticles, a molarity of 1 M in the final mixture was used for all Itz/P407/HPMC samples. The excess salinity (above the minimum required, 0.25 M) ensured strong attractive forces between the polymer chains. In both cases the flocculation was essentially instantaneous, in less than 1 s after mixing the salt solutions (Fig. 1B), indicating loss of the steric stabilization by the PEO chains. Average floc sizes were ~5–7 μm, according to microscopic observation just after mixing with salt solution, shown in Fig. 2. Figure 1B shows the large flocculated particles took up the entire dispersion volume, and creaming of the flocs reached steady state in 3 min (Fig. 1C). Spontaneous redispersion occurred upon regaining good solvent quality by adding the dried powders to pure water with gentle stirring (Fig. 1D).

The sodium sulfate concentration in the filtrate after rinsing with 30 ml of the HPMC solution was verified using conductivity and in all cases, the weight of salt removed in the filtrate was more than 90% of the total salt added. As a result, the final powders from the filter cake contained less than 1% Na_2SO_4 by weight. HPLC analysis of the filtrate also showed no more than 3% (drug wt. in filtrate/tot. wt. drug) of the drug was lost through the filter, indicating yields higher than 97% *w*/*w*. The residual salt in the final dried powder corresponded to less than 2.5 mg per 200 mg dose of Itz (based on 90% drug loading). This quantity is well below the 120 mg of Na_2SO_4 allowed in an oral dosage form, according to the inactive ingredient guide published by the FDA.

Filtration rates of the Itz dispersions, reported in Table I, were similar to those of flocculated naproxen nanoparticle suspensions in a previous study (32,33). In all formulations, free polymer, which was not bound to drug particles, was removed with the filtrate, producing drug loadings typically around 90% *w*/*w*, as tabulated in Tables I and II. Polymer loading was determined by a simple mass balance and reported as % *w*/*w*. Extremely high filtration selectivities for drug particles over polymer, (g drug precipitate/g drug filtrate)/(g polymer precipitate/g polymer filtrate) were observed, as reported in Table I, and were similar to values reported by the flocculation of naproxen (32,33).

Table I. Properties of Salt Flocculation of HPMC-stabilized Suspensions

Sample	Na_2SO_4 molarity to flocculate	Filtration rate (ml/cm^2 min)	Drug lost in filtrate (% drug wt./ tot. drug wt.)	Drug loading (% *w*/*w*)	Drug yield (% drug wt./tot. drug wt.)	Salt (% *w*/*w*)	Polymer (% *w*/*w*)	Selectivity
A—4:1 Itz/HPMC	0.25	0.101	1.1	92±0.3	95.4	0.63	7.4	200±17
B—2:1 Itz/HPMC	0.25	0.089	2.9	90±0.1	89.0	0.27	9.7	130±23
C—1:1 Itz/HPMC	0.3	0.093	0.30	94±0.7	101	0.81	5.2	6,300±1,000

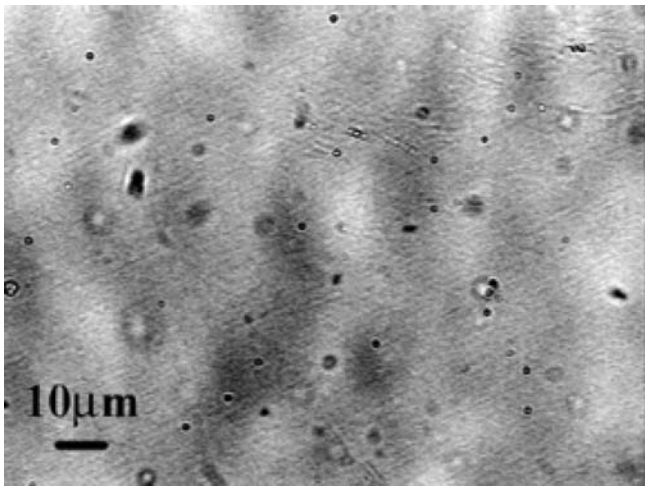

Fig. 2. Optical microscopy of 8:1:2 Itz/P407/HPMC dispersion just after addition of salt solution.

Particle Morphology After Flocculation and Filtration

Using light scattering, particle sizes were measured after removal of organic solvent from the precipitated dispersions and after redispersion of dried powders into water. Without the use of P407 as a stabilizer, particle sizes of aqueous dispersions just after organic solvent removal were large (1–5 μm diameters), despite dried powder surface areas as high as 51 m^2/g, measured in a previous study (7). Addition of P407 to the formulation mitigated agglomeration of nanoparticles during antisolvent precipitation and light scattering measurements, prior to addition of salt, gave sizes in the submicron range. Increasing the P407 concentration led to a decrease in average particle size until a threshold was reached at approximately 300 nm, shown in Table II. This trend has been observed in previous studies where the ratio of the mixing time and precipitation time, the dimensionless Damkohler number, was decreased by either increasing stabilizer concentration (18) or mixing energy (23). The particle size decreased until a plateau was reached where the Damkohler number was <1.

As listed in Table II, the average sizes of P407/HPMC systems after redispersion were typically within 40 nm of the original dispersion before flocculation. For rapidly frozen and lyophilized 8:1:2 Itz/P407/HPMC, the average size after redispersion was 700 nm, over twice the original value, see Table II. The spray dried 8:1:2 Itz/P407/HPMC average size was quite large, 5 μm, after redispersion. Contact angles (reported Table II) of all salt flocculated samples, including the homogenized control, were all approximately 20–40° regardless of the formulation. The rapidly frozen and lyophilized control had a much higher angle of 51°. Pure Itz and HPMC had contact angles of 79° and 66°, respectively.

Modulated DSC of formulations A–C revealed the presence of two glass transitions, one for Itz (~58°C (45)) and HPMC (~154°C (45)) as seen in Fig. 3. These two T_gs indicated two distinct phases in the drug nanoparticles. Previous work with precipitated Itz/HPMC systems established a core-

Table II. Drug Loading, Original Particle Size, Particle Size after Redispersion, Contact Angle with pH 6.8 Media, and $AUC_{2\ h}$ of Salt Flocculated HPMC/P407-stabilized Itz Dispersions

Itz/P407/HPMC ratio	Theoretical drug loading (% *w*/*w*)	Drug loading after flocculation (% *w*/*w*)	Size before flocculation (D10/D50/D90) μm	Size after redispersion and 5 min sonication (D10/D50/D90) μm	Average θ	Supersat. $AUC_{2\ h}$
D—32:1:8 salt flocculated	78	87±1.2	0.12/1.27/3.04	0.16/0.79/2.72	19±3.7	768
E—8:1:2 salt flocculated	73	94	0.11/0.34/2.26	0.12/0.37/1.48	23±6.8	663
F—4:1:1 salt flocculated	67	80±3.6	0.11/0.29/1.08	0.12/0.33/1.09	38±2.5	548
G—8:3:2 salt flocculated	61	88	0.11/0.29/2.28	0.11/0.31/0.97	33±3.2	404
H—8:1:2 homogenized and salt flocculated	73	90±2.0	0.20/0.68/1.65	0.21/0.81/1.81	31±6.8	NA
I—8:1:2 rapidly frozen, not salt flocculated	73	NA	0.11/0.28/0.80	0.14/0.70/5.80	51±3.3	NA
J—8:1:2 suspension, no drying	73	NA	0.11/0.34/2.26	NA	NA	1,120
K—8:1:2 spray dried	73	NA	0.11/0.34/2.26	0.27/5.18/10.8	NA	NA
L—8:1:2 dispersion, slowly heated	73	NA	0.11/0.34/2.26	2.30/5.96/40.1	NA	NA
M—8:1:2 dispersion, rapidly heated	73	NA	0.12/0.19/0.34*	0.17/0.23/0.31*	NA	NA

Na_2SO_4 molarity after mixing salt solution and dispersion was 1 M in all cases. *Sizes were measured with static light scattering, except formulation M where dynamic light scattering was used

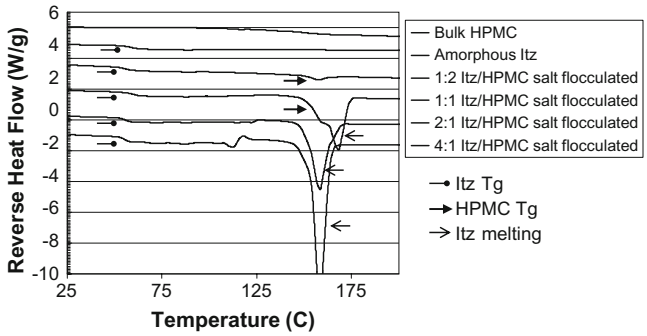

Fig. 3. Reversible heat flow from modulated differential scanning calorimetry: HPMC-stabilized, salt flocculated powders.

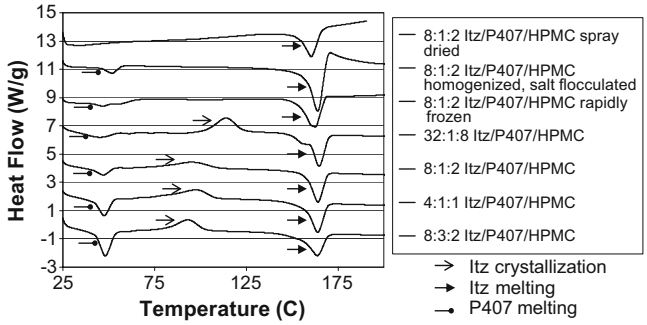

Fig. 5. Heat flow from modulated differential scanning calorimetry: HPMC/P407-stabilized, salt flocculated powders and spray dried, homogenized, and rapidly frozen controls.

shell arrangement of drug and polymer, as evident from surface content analysis via X-ray photoelectron microscopy and contact angle measurements (7). As the polymer is water soluble, its adsorption to the surface of precipitated hydrophobic surfaces orients the polymer primarily to the surface of the particles, lowering the interfacial energy of the system. This surface orientation facilitates the use of very little polymer to stabilize nanoparticles with high drug loading.

In addition to hydrophilic polymers, excess salt was detected on the surface of dried particles by contact angle measurements with pH 6.8 buffer. Contact angles of salt flocculated powders, including the homogenized sample, were much lower than for both pure Itz (79±13°) and HPMC (66±3.9°) alone. For the lyophilized control, it was lower than that of pure HPMC from the presence of P407 on the surface, but still higher than those of the flocculated samples. The more favorable wetting for the flocculated particles has the potential to accelerate dissolution.

The crystallization of amorphous drug during mDSC heating was evident in an exothermic peak ranging from 90° to 130°, as shown in Figs. 4 and 5. The crystallization temperature increased with HPMC content, Fig. 4, and decreased with P407 content, Fig. 5. The change in kinetics of crystallization may be explained by a decrease in mobility with an increase in HPMC and an increase with P407. Melting peaks of the *in situ* crystallized drug are observed in both Figs. 4 and 5, at ~168°C. In Fig. 3, the melting peak of Itz overlapped with the T_g peak for HPMC. In Fig. 5, the melting peak for P407 can also be seen at ~45°C, which masked the T_g of Itz. In all cases the presence of a glass transition for Itz and/or a crystallization peak verified the amorphous character of flocculated, dried powders. Homogenized, rapidly frozen, and spray dried 8:1:2 Itz/P407/HPMC controls, (Table II; formulations H, I, and K, respectively), exhibited no evidence of amorphous drug as there was no crystallization peak, but a large melting peak at ~168°C.

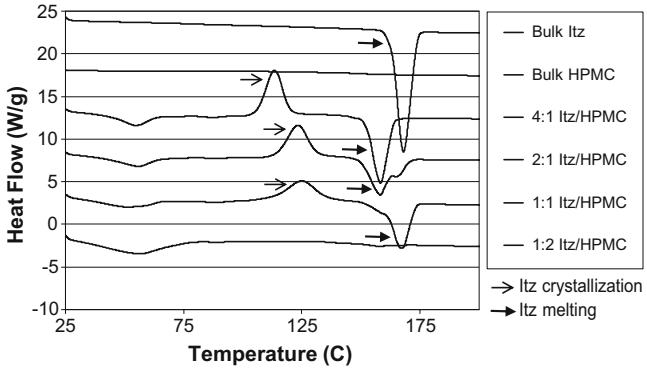

Fig. 4. Heat flow from modulated differential scanning calorimetry: HPMC-stabilized, salt flocculated powders.

Dissolution of Flocculated Nanoparticles Under Supersaturated Conditions

The supersaturation curves and the calculated areas under the curve (AUC) are shown in Fig. 6 and Table II, respectively. In the case of dried powders, an amount equal to 25-times the equilibrium solubility was added at time zero. For the 8:1:2 Itz/P407/HPMC original nanoparticle dispersion, drops were added slowly to minimize excess particles, which would otherwise facilitate heterogeneous nucleation. It has been shown recently that the supersaturation produced by this technique may approach the metastable solubility limit in pH 6.8 buffer with 0.17% SDS (7). The maximum in the supersaturation level for salt flocculated, dried powders was ~14, even greater than that for the original nanoparticle dispersion (shown in Fig. 6). Dissolution rates were rapid for all supersaturation curves, as expected from high surface areas and a large driving force from the high metastable

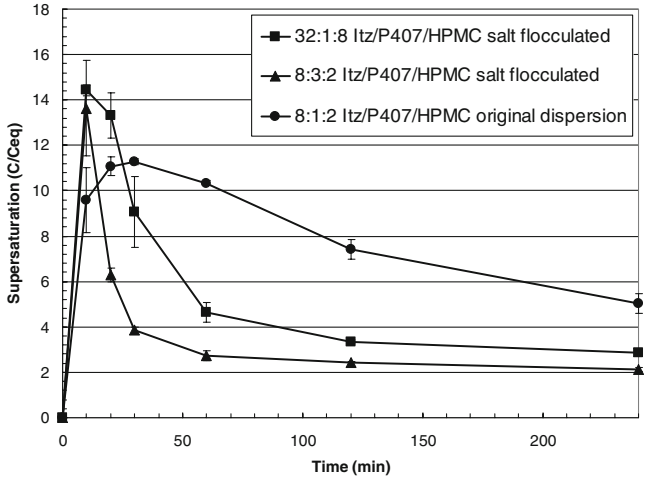

Fig. 6. Supersaturation *versus* time of salt flocculated powders in pH 6.8 media with 0.17% SDS, compared with lyophilized and original dispersion before flocculation.

solubility. For flocculated samples, however, the supersaturation decayed more rapidly than for the 8:1:2 Itz/P407/HPMC dispersion. The supersaturation can be reduced by incorporation of the dissolved ITZ into the excess particles. The slower decay in supersaturation, and consequently, larger AUC for the original dispersion is likely caused by the lack of excess solid particles. Similarly, the larger (lower surface area/volume) excess particles in the 32:1:8 flocculated sample may explain its larger AUC relative to the other three flocculated samples.

The lyophilized samples crystallized as a result of high mobility during water sublimation caused by the low T_g P407. Since crystallization of drug occurred in both the rapidly frozen/lyophilized and spray dried 8:1:2 Itz/P407/HPMC controls, as evident by mDSC in Fig. 5, dissolution experiments were not performed. Thus the lack of crystallization in the salt flocculation process is a significant advantage.

DISCUSSION

Flocculation of Sterically Stabilized Dispersions by Salt

The lowering of the cloud point temperature of PEO or HPMC with electrolytes has received significant attention (35,36,44). Structural incompatibility of the hydrophilic hydration layer about the ether oxygen atoms of PEO with anion-associated water molecules leads to desolvation of the polymer chains (46,47). As the polymer chains are desolvated, the segmental interactions of polymer chains become attractive and the chains collapse (29,30). For colloids with adsorbed PEO, the interparticle attractive forces of the desolvated polymer layer cause flocculation of the particles (33,40,42,48–50).

For rapid diffusion limited Smoluchowski flocculation, in the limit of no stabilization, each collision is sticky (30) and the rate of change in number of particles is given by:

$$r_s = k_s n_p^2 \tag{1}$$

where n_p is number of particles per volume (ml^{-1}) and k_s is calculated from the temperature and kinematic viscosity of the medium (30). Under very poor solvent conditions, flocculation for PEO stabilized particles (51,52) is rapid, and the stability ratio, that is, r_s/actual rate, is close to 1. For PEO stabilized colloids (50–52), the solvent quality has been varied by raising temperature to achieve stability ratios of 2.3.

The ratio of particle diameter to stabilizing polymer layer, a/δ, may be used to delineate the importance of van der Waals core–core *versus* polymer–polymer interactions. In our study, particles sizes of ~300 nm with an adsorbed PEO layer of ~15 nm in length have relatively thick polymer layers, where a/δ=20 (53). For poor solvent conditions, the collapsed polymer layers produce strong attractive forces between the particles, whereas the core-core attraction is minor. Excess salt was added to the dispersions, above the minimum critical flocculation concentration to produce strong attractive forces and rapid flocculation seen in Fig. 1. For a stability ratio approaching unity, Eq. 1 predicts the number density of particles will be reduced by half after only 0.11 s for n_p was $\sim 1.4\times10^{12}$ ml^{-1}, in good agreement with the instantaneous flocculation observed visually. The flocculation rates could not be measured directly with light scattering, since the flocculation was so rapid and the dispersions were extremely turbid.

The floc structure depends on both the interparticle forces and the volume fraction of particles, ϕ, as illustrated by the schematic in Fig. 7 (28,30,54,55). Immediately after the addition of excess salt, ϕ in pathway A is essentially constant, prior to creaming, as the volume of the aqueous dispersion remains constant. Here, the rapid generation of strong interparticle attractive forces forms an interconnected network with a loose, open fractal structure (pathway A in Fig. 7). As shown in Table II and the SEMs of Fig. 8, the particles redispersed to their original size in good solvent conditions, behavior indicative of loose flocs. The very small 300 nm primary particles diffuse rapidly and bind to a primary particle already on the growing floc. The strong attraction inhibits significant rearrangement of the loose floc to minimize surface area, preserving an open floc (28,30,54,55).

The fractal dimension of a floc, D_f, characterizes the floc structure by relating the volume fraction of solid in the floc, ϕ_k to the primary particle diameter, d, and the floc diameter, d_k (28):

$$\phi_k = \left(\frac{d_k}{d}\right)^{D_f-3}. \tag{2}$$

For a floc composed of densely packed particles, D_f approaches 3. For more open structures, or fractals produced by rapid diffusion-limited aggregation, D_f is typically ~1.7 (28). As shown in Fig. 1D, 3 min after addition of salt solution, the flocs creamed to a steady state volume. Assuming the flocs are at the closest packed density in this cream layer, ϕ_k can be assumed to be approximately equal to ϕ in the cream layer. The cream layer volume was approximately half the volume of the original dispersion, shown in Fig. 1A, indicating ϕ increased from 0.01 to 0.02. Based on the measured values of d=300 nm and d_k=7 μm, D_f is approximately 1.76 for salt flocculated Itz/P407/HPMC dispersions, representative of an open floc. With D_f<<3, the flocs are loose and open in structure (28) consistent with the essentially complete redispersion once good solvent conditions are reestablished, as shown in Table II.

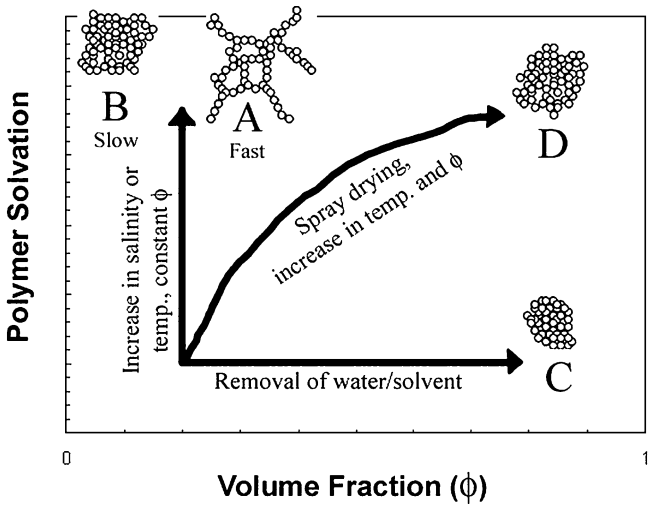

Fig. 7. Floc structure as a function of polymer solvation and ϕ. Polymer solvency diminishes with an increase in salinity or temperature.

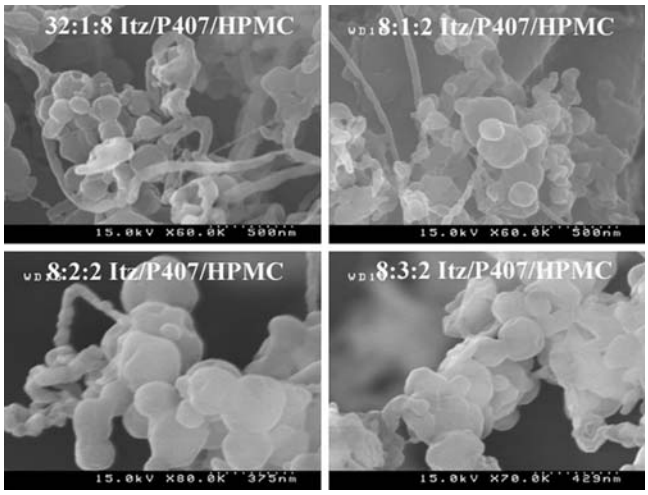

Fig. 8. SEM of salt flocculated Itz dispersions after rapid freezing onto aluminum stage.

Upon returning the thick (a/δ=20) stabilizing polymer to good solvent conditions, the weak attractive forces between particle cores is easily overcome by the solvation of the polymer chains. In the flocculated state, hydrogen bonding between PEO chains is relatively weak, due to only one terminal hydrogen bond donor group per chain. With the low melting point of PEO, reflecting weak intermolecular forces, the collapsed chains are non-crystalline, and are easily solvated upon redispersion in water. The primary particles in the open flocs are highly accessible to the solvent with high surface area. Also, the residual salt in the final powder was sufficiently low to allow full solvation of stabilizing moieties. Thus the solvation of the thick polymer layers on the accessible particles in the open flocs with low residual salt leads to essentially complete redispersion to the original particle size of 300 nm.

Comparison of Flocculation and Filtration to Other Separation Techniques

During mixing of salt solution with the nanoparticle dispersion, the overall volume of the system increases, decreasing ϕ from ~0.01 to 0.003, as the flocs take up the entire dispersion volume (Fig. 1B). Immediately after mixing, the flocculation takes place under very dilute and constant ϕ conditions, as shown by pathway A in Fig. 7, to form loose open flocs. Filtration removes water and solvent in a separate step after the floc is formed. In contrast, ϕ increases continually in freezing processes as the water and/or organic solvents are frozen (pathway C, Fig. 7). ϕ_k must be equal to or greater than ϕ, therefore the removal of water and/or solvent increases the minimum possible floc density. The maximum value of ϕ is 0.74, assuming close packed spheres. Based on Eq. 2, with d=280 nm and d_k=700 nm (Table II) from rapidly frozen 8:1:2 Itz/P407/HPMC, an increase in ϕ_k from 0.01 to 0.74 gives an increase in D_f from 2.4 to 2.96 (reported in Table III). The high fractal dimension suggests a much more densely packed floc formed by rapid freezing than salt flocculation, consistent with much larger particle sizes upon redispersion of the former.

Slowly heating the 8:1:2 Itz/P407/HPMC nanoparticle dispersion to 92°C, at relatively constant ϕ with limited evaporation (pathway B, Fig. 7), resulted in slow, irreversible flocculation, as the particles redispersed at ambient temperature to a large size of ~5 μm even with sonication (Table II). Since 92°C is just below the cloud point of PEO in water (~100°C (36)), flocculation was slow from weak attractive forces of only partially collapsed polymer layers (53). In contrast, dispersions of 300 nm 8:1:2 Itz/P407/HPMC particles were heated rapidly just to the cloud point temperature at 98°C, under constant ϕ conditions (pathway A, Fig. 7). Rapid heating without evaporation formed open flocs which redispersed to their original size upon cooling (Table II). Bevan and Prieve also showed reversible flocculation from rapid heating of PEO-stabilized polystyrene latex spheres (50–52). Thus, the rate of change in PEO solvency directly impacts the structure of the floc, as indicated by its size upon redispersion in water.

During spray drying, the evaporation of water causes a marked increase in ϕ simultaneously with an increase in temperature, as shown by pathway D in Fig. 7. Since the dispersion is heated to 140°C, much higher than the cloud point of PEO, the polymer becomes desolvated. Heating of the ~20 μm high surface area droplets occurs in milliseconds, as evident by the fact that droplets evaporate before hitting the side walls of the spray dryer. The rapid rate of heating and thus, desolvation of the thick stabilizer shell, produces strong attractive forces between the particles. However, with the simultaneous increase in ϕ, the flocs become densely packed, and may be further compressed by the large capillary forces of the shrinking droplets. Thus the aggregates do not redisperse to the primary particle size, as reported in Table II. The final particle size can be estimated by assuming all particles present in the initial droplet create a single larger particle upon water evaporation (56). Under the conditions of spray drying as detailed above, droplets are 10–30 μm, based on measurements made by Engstrom (57). With an initial particle concentration of 10 mg/ml and a particle density of

Table III. Estimated Values of Fractal Dimension for Upper and Lower Limits of Volume Fraction of Solid in the Floc According to Eq. 2

Salt flocculated		Rapidly frozen		Spray dried	
d_k/d=7 μm/300 nm		d_k/d=700 nm/280 nm		d_k/d=5 μm/300 nm	
ϕ_k	D_f	ϕ_k	D_f	ϕ_k	D_f
0.003	1.2	0.01	2.4	0.01	1.4
0.02	1.8	0.67	3.0	0.67	2.9

1.3 g/cm^3 (based on the bulk drug density), a single particle of 4.4 μm would be produced from each 20 μm drop, assuming closest packed spheres. This value is very close to the experimental particle size of 5 μm upon redispersion. As reported in Table III, when ϕ is assumed to be 0.74, the closest packed limit, the fractal dimension of the flocs is approximately 2.90, indicative of densely packed flocs. Therefore, the ability to maintain a low nearly constant value of ϕ in the salt flocculation process is highly advantageous for producing open flocs which are highly redispersible, unlike the denser flocs produced by the freezing and spray drying processes where ϕ increased markedly.

Increase in Drug Loading by Flocculation and Filtration

In addition to forming a redispersible floc, salt flocculation and filtration also offers the advantage of removing excess polymer from the final powder, as is evident from the increase in drug loadings reported in Tables I and II. As the large, flocculated particles are trapped on top of the filter, free unadsorbed polymer escapes with the filtrate. Although the free polymer is also desolvated by salt and forms a collapsed structure, its effective diameter is on the order of 10 nm, based on measured PEO coil lengths under poor solvent conditions (53). Since the concentrations of polymer in solution are low, approximately 1.67 mg/ml (P407) and 2.5 mg/ml (HPMC), the collapsed free polymers were not likely to flocculate to high enough diameters to be trapped by the filter paper with 1–5 μm pores. Additionally, in a control experiment, pure polymer solutions of 1.67 mg/ml P407 and 2.5 mg/ml HPMC were flocculated with 1 M Na_2SO_4 and passed through the filter to produce a cloudy filtrate with minimal polymer on the filter paper. For polymer stabilized dispersions, the high selectivity for particles *versus* free polymer during filtration is evident from the large values (150–6,300) reported in Table I. During solution precipitation, as well as milling processes, to form nanoparticles a high concentration of polymer in solution is highly beneficial for generating a large driving force for adsorption to particle surfaces to inhibit particle growth (30). Once the particles are formed and passivated with the stabilizer, our results indicate that the unbound polymer is no longer needed and can be removed without further particle growth.

Preservation of Amorphous Drug by Flocculation and Filtration

Flocculation and filtration were performed at low temperatures to minimize particle growth and crystallization of the drug. As observed in mDSC thermograms, temperatures as low as 90°C lead to the crystallization of amorphous Itz. Spray drying, which requires temperatures in this range (57,58), caused crystallization of the amorphous precipitated particles, as shown by the single melting peak of Itz in Fig. 5. For salt flocculation, the rapid filtration at low temperatures mitigated crystallization as was evident in mDSC and supersaturation experiments. Spray drying forces particles close together as the water is removed by evaporation or ice formation and the concentration of free excipients also increases. Both of these factors enhance the rate of particle growth and crystallization.

When one or both of the polymers exhibits a low T_g, such as P407, removal of the excess polymer with filtration can reduce crystallization tendency of the drug. As shown in the mDSC thermograms in Fig. 5, the crystallization temperature of amorphous Itz decreased with increasing P407 content. P407 melts around 50°C, where Itz can dissolve in the molten polymer, resulting in solvent-mediated crystallization of drug. In contrast, the higher T_g polymer, HPMC, increased the crystallization temperature, as apparent in the mDSC curves in Fig. 4. According to the Gordon Taylor equation (59,60), the fraction of high T_g material may be determined to achieve a reasonable composite T_g. Also, removal of excess polymer (including low T_g material) in the final powder by filtration is beneficial for the storage stability of amorphous nanoparticles. At low temperatures, rapid removal of solvent and excess low T_g polymer immediately after precipitation, flocculation, and filtration, helps maintain an amorphous state, in contrast to spray drying where high temperatures and concentration of the particles and free excipients caused crystallization.

Dissolution of Flocculated Particles to Produce Supersaturated Solutions

The rate of dissolution has been shown to influence the maximum level of supersaturation (7). The undissolved solid is susceptible to solvent-mediated crystallization during the dissolution process, upon contact with water. In our previous study, amorphous pure Itz particles were dissolved in acidic media and the maximum supersaturation levels were correlated to the surface area available for dissolution (7). Rapidly dissolving amorphous nanoparticles have less time to crystallize in the presence of dissolution media. In an ensuing study (Matteucci *et al.*, in preparation), pre-wet Itz particles in suspension created the highest supersaturation levels, which were close to the theoretical solubility predicted by a heat capacity corrected Gibbs free energy difference between the amorphous and crystalline drug (4,5). Likewise, the rapidly dissolving salt flocculated powders produced supersaturation levels approaching the metastable solubility limit, as estimated by dropwise addition of the nanoparticle dispersion (without salt flocculation) to pH 6.8 media (Fig. 6). In contrast, dissolution of low surface area amorphous Itz made by solvent evaporation with HPMC only generated supersaturation levels up to 2.5 in pH 6.8 media. (Matteucci *et al.*, in preparation) Therefore, the high surface area, polymer coated, amorphous particles formed by the salt flocculation process produce much higher supersaturation levels than low surface area solid dispersions.

CONCLUSIONS

The simple flocculation/filtration process may be used to recover nanoparticles from aqueous dispersions rapidly and efficiently, with yields on the order of 90%, while maintaining amorphous primary particles that may be dissolved in aqueous media to achieve high supersaturation levels. Addition of salt to polymer-stabilized amorphous nanoparticle dispersions collapsed the stabilizer chains to produce large flocs which were filtered rapidly. Large amounts of stabilizers may be used in the particle formation stage to minimize particle growth, and then excess stabilizer may be removed in

the filtration step to achieve high drug loadings up to 90%. The rapid change in interparticle forces, under constant particle volume fraction (ϕ), produced open flocs (low fractal dimension) and excellent redispersion in water to the original particle size of 300 nm. In contrast, drying of nanoparticle dispersions by either spray drying or rapid freezing/lyophilization produced densely packed flocs (high fractal dimension), which did not redisperse to form submicron particles.

For the salt flocculation/filtration process, the low temperature and constant dilute ϕ conditions, as well as rapid removal of solvent, inhibited both growth and crystallization of the amorphous primary nanoparticles. High supersaturation levels up to 14-times the crystalline solubility in pH 6.8 media were facilitated by rapid dissolution of the nanoparticles prior to crystallization in the presence of the media. High supersaturation levels would have the potential to improve absorption markedly of poorly water soluble drugs in the gastrointestinal tract. However, for particles produced by spray drying, the increase in ϕ and high temperature led to crystallization of the nanoparticles and with yields well below the values of 90% in the flocculation/filtration process. The ability to recover nanoparticles from aqueous dispersions rapidly by forming loose flocs, which are readily redispersible to the original particle size, and without the need to evaporate the water, is of general interest for all types of nanoparticles including pharmaceuticals.

ACKNOWLEDGMENTS

We gratefully acknowledge the financial support from The Dow Chemical Company (Midland, MI). This material is based upon work supported in part by the STC Program of the National Science Foundation under Agreement No. CHE-9876674 and the Welch Foundation.

REFERENCES

1. C. A. Lipinski. Poor aqueous solubility—an industry wide problem in drug discovery *Am. Pharm. Rev.* **5**:82–85 (2002).
2. S. L. Raghavan, B. Kiepfer, A. F. Davis, S. G. Kazarian, and J. Hadgraft. Membrane transport of hydrocortisone acetate from supersaturated solutions; the role of polymers. *Int. J. Pharm.* **221**:95–105 (2001).
3. U. Kumprakob, J. Kawakami, and I. Adachi. Permeation enhancement of ketoprofen using a supersaturated system with antinucleant polymers. *Biol. Pharm. Bull.* **28**:1684–1688 (2005).
4. B. C. Hancock, and M. Parks. What is the true solubility advantage for amorphous pharmaceuticals? *Pharm. Res.* **17**:397–404 (2000).
5. P. Gupta, G. Chawla, and A. K. Bansal. Physical stability and solubility advantage from amorphous celecoxib: The role of thermodynamic quantities and molecular mobility. *Mol. Pharmaceutics.* **1**:406–413 (2004).
6. G. S. Parks, L. J. Snyder, and F. R. Cattoir. Studies on glass. XI. Some thermodynamic relations of glassy and alpha-crystalline glucose. *J. Chem. Phys.* **2**:595–598 (1934).
7. M. E. Matteucci, B. K. Brettmann, T. L. Rogers, E. J. Elder, R. O. Williams III, and K. P. Johnston. Design of potent amorphous drug nanoparticles for rapid generation of highly supersaturated media. *Mol. Pharmaceutics.* **4**:782–793 (2007).
8. T. Yamada, N. Saito, T. Imai, and M. Otagiri. Effect of grinding with hydroxypropyl cellulose on the dissolution and particle size of a poorly water-soluble drug. *Chem. Pharm. Bull.* **47**:1311–1313 (1999).
9. K. Yamashita, T. Nakate, K. Okimoto, A. Ohike, Y. Tokunaga, R. Ibuki, K. Higaki, and T. Kimura. Establishment of new preparation method for solid dispersion formulation of tacrolimus. *Int. J. Pharm.* **267**:79–91 (2003).
10. A. Hasegawa, R. Kawamura, H. Nakagawa, and I. Sugimoto. Physical properties of solid dispersions of poorly water-soluble drugs with enteric coating agents. *Chem. Pharm. Bull.* **33**:3429–3435 (1985).
11. G. Verreck, K. Six, G. Van den Mooter, L. Baert, J. Peeters, and M. E. Brewster. Characterization of solid dispersions of itraconazole and hydroxypropylmethylcellulose prepared by melt extrusion—part I. *Int. J. Pharm.* **251**:165–174 (2003).
12. K. Okimoto, M. Miyake, R. Ibuki, M. Yasumura, N. Ohnishi, and T. Nakai. Dissolution mechanism and rate of solid dispersion particles of nilvadipine with hydroxypropylmethylcellulose. *Int. J. Pharm.* **159**:85–93 (1997).
13. H. Suzuki, and H. Sunada. Comparison of nicotinamide, ethylurea and polyethylene glycol as carriers for nifedipine solid dispersion systems. *Chem. Pharm. Bull.* **45**:1688–1693 (1997).
14. Y. Zhu, N. Shah, H. A. W. Malick, M. H. Infeld, and J. W. McGinnity. Controlled release of a poorly water-soluble drug from hot-melt extrudates containing acyrlic polymers. *Drug Dev. Ind. Pharm.* **32**:569–583 (2006).
15. C. Aitken-Nichol, F. Zhang, and J. W. McGinnity. Hot melt extrusion of acrylic films. *Pharm. Res.* **13**:804–808 (1996).
16. G. Sertsou, J. Butler, J. Hempenstall, and T. Rades. Solvent change co-precipitation with hydroxylpropyl methylcellulose phthalate to improve dissolution characteristics of a poorly water-soluble drug. *J. Pharm. Pharmacol.* **54**:1041–1047 (2002).
17. J. Huang, R. J. Wigent, C. M. Bentzley, and J. B. Schwartz. Nifedipine solid dispersion in microparticles of ammonio methacrylate copolymer and ethylcellulose binary blend for controlled drug delivery: Effect of drug loading on release kinetics. *Int. J. Pharm.* **319**:44–54 (2006).
18. M. E. Matteucci, M. A. Hotze, R. O. Williams III, and K. P. Johnston. Drug nanoparticles by antisolvent precipitation: Mixing energy *versus* surfactant stabilization. *Langmuir.* **22**:8951–8959 (2006).
19. G. Muhrer, U. Meier, F. Fusaro, S. Albano, and M. Mazzotti. Use of compressed gas precipitation to enhance the dissolution behavior of a poorly water-soluble drug: Generation of drug microparticles and drug-polymer solid dispersions. *Int. J. Pharm.* **308**:69–83 (2006).
20. E. M. Liversidge, G. G. Liversidge, and E. R. Cooper. Nanosizing: A formulation approach for poorly-water-soluble compounds. *Eur. J. Pharm. Sci.* **18**:113–120 (2003).
21. R. H. Muller, and B. H. L. Bohm. *Nanosuspensions*, Colloidal Drug Carriers Expert Meeting, Berlin, 1997, pp. 149–174.
22. C. Jacobs, O. Kayser, and R. H. Muller. Nanosuspensions as a new approach for the formulation for the poorly soluble drug tarazepide. *Int J Pharm.* **196**:161–164 (2000).
23. B. K. Johnson. *Flash Nanoprecipitation of Organic Actives via Confined Micromixing and Block Copolymer Stabilization*. Department of Chemical Engineering, Princeton, 2003.
24. D. Horn, and E. Luddecke. Preparation and characterization of nano-sized carotenoid hydrosols. *NATO ASI Ser. 3: High Technol.* **12**:761–775 (1996).
25. T. L. Rogers, I. B. Gillespie, J. E. Hitt, K. L. Fransen, C. A. Crowl, C. J. Tucker, G. B. Kupperblatt, J. N. Becker, D. L. Wilson, C. Todd, C. F. Broomall, J. C. Evans, and E. J. Elder. Development and characterization of a scalable controlled precipitation process to enhance the dissolution of poorly water-soluble drugs. *Pharm. Res.* **21**:2048–2057 (2004).
26. N. Rasenack, and B. W. Muller. Dissolution rate enhancement by *in situ* micronization of poorly water-soluble drugs. *Pharm. Res.* **19**:1894–1900 (2002).
27. J. D. Holmes, K. P. Johnston, R. C. Doty, and B. A. Korgel. Control of thickness and orientation of solution-grown silicon nanowires. *Science*. **287**:1471–1473 (2000).
28. R. G. Larson. *The Structure and Rheology of Complex Fluids*. Oxford University Press, New York, 1999.
29. D. H. Napper. *Polymeric Stabilization of Colloidal Dispersions*. Academic, New York, 1983.
30. P. C. Heimenz, and R. Rajagopalan. *Principles of Colloid and Surface Chemistry*. Marcel Dekker, New York, 1997.

31. I. Limayem, C. Charcosset, and H. Fessi. Purification of nanoparticle suspensions by a concentration/diafiltration process. *Separation and Purification Technology.* **38**:1–9 (2004).
32. X. Chen, M. E. Matteucci, C. Y. Lo, R. O. Williams, III, and K. P. Johnston. Flocculation of suspensions formed by antisolvent precipitation to produce redispersible naproxen nanocrystals. *Drug Dev. Ind. Pharm*. (in press).
33. X. Chen. *Nanoparticle Engineering Processes: Evaporative Precipitation into Aqueous Solution (EPAS) and Antisolvent Precipitation to Enhance the Dissolution Rates of Poorly Water Soluble Drugs.* Department of Chemical Engineering. University of Texas, Austin, 2004.
34. V. S. Murthy, J. N. Cha, G. D. Stucky, and M. S. Wong. Charge-driven flocculation of poly(L-lysine)-gold nanoparticle assemblied leading to hollow microspheres. *J. Am. Chem. Soc.* **126**:5292–5299 (2004).
35. N. Pandit, T. Trygstad, S. Croy, M. Bohorquez, and C. Koch. Effect of salts on the micellization, clouding, and solubilization behavior of pluronic F127 solutions. *J. Colloid Interface Sci.* **222**:213–220 (2000).
36. P. Pang, and P. Englezos. Phase separation of polyethylene oxide (PEO)-water solution and its relationship to the flocculating capability of the PEO. *Fluid Phase Equilib.* **194–197**:1059–1066 (2002).
37. P. Bahadur, P. Li, M. Almgren, and W. Brown. Effect of potassium fluoride on the micellar behavior of Pluronic F-68 in aqueous solution. *Langmuir.* **8**:1903–1907 (1992).
38. P. Bahadur, K. Pandya, M. Almgren, P. Li, and P. Stilbs. Effect of inorganic salts on the micellar behavior of ethylene oxide-propylene oxide block copolymer in aqueous solution. *Colloid Polym. Sci.* **271**:657–667 (1993).
39. P. Alexandridis, and J. F. Holzwarth. Differential scanning calorimetry investigation of the effect of salts on aqueous solution properties of an amphiphilic block copolymer (poloxamer). *Langmuir.* **13**:6074–6082 (1997).
40. D. H. Napper. *Colloid and Interface Science*. Academic, New York, 1977.
41. R. H. Pelton. Polystyrene and polystyrene-butadiene latexes stabilized by poly(N-isopropylacrylamide). *J. Polym. Sci., A, Polym. Chem.* **26**:9–18 (1988).
42. C.-W. Chen, D. Tano, and M. Akashi. Colloidal platinum nanoparticles stabilized by vinyl polymers with amide side chains: Dispersion stability and catalytic activity in aqueous electrolyte solutions. *J. Colloid Interface Sci.* **225**:349–358 (2000).
43. N. Nyamweya, and S. W. Hoag. Assessment of polymer-polymer interactions in blends of HPMC and film forming polymers by modulated temperature differential scanning calorimetry. *Pharm. Res.* **17**:625–631 (2000).
44. X. M. Xu, Y. M. Song, Q. N. Ping, Y. Wang, and X. Y. Liu. Effect of ionic strength on the temperature-dependent behavior of hydroxypropyl methylcellulose solution and matrix tablet. *J. Appl. Polym. Sci.* **102**:4066–4074 (2006).
45. K. Six, H. Berghmans, C. Leuner, J. Cressman, K. Van Werde, J. Mullens, L. Benoist, M. Thimon, L. Meublat, G. Verreck, J. Peeters, M. E. Brewster, and G. Van den Mooter. Characterization of solid dispersions of itraconazole and hydroxypropylmethylcellulose prepared by melt extrusion, part II. *Pharm. Res.* **20**:1047–1054 (2003).
46. I. D. Robb. *The Chemistry and Technology of Water Soluble Polymers*. Plemun, London, 1982.
47. D. Eagland. *Water*. Plenum, New York, 1975.
48. D. H. Napper. Steric stabilization and the hofmeister series. *J. Colloid Interface Sci.* **33**:384–392 (1970).
49. D. H. Napper. Flocculation studies of sterically stabilized dispersions. *J. Colloid Interface Sci.* **32**:106–114 (1970).
50. M. A. Bevan, and P. J. Scales. Solvent quality dependent interactions and phase behavior of polystyrene particles with physisorbed PEO-PPO-PEO. *Langmuir.* **18**:1474–1484 (2002).
51. M.A. Bevan. *Effect of Adsorbed Polymer on the Interparticle Potential*. Department of Chemical Engineering. Carnegie Mellon University, Pittsburgh, 1999.
52. D. C. Prieve, and M. A. Bevan. *Polymers in Particulate Systems: Properties and Applications*. Marcel Dekker, New York, 2002.
53. M. A. Bevan, and D. C. Prieve. Forces and hydrodynamic interactions between polystyrene surfaces with adsorbed PEO-PPO-PEO. *Langmuir.* **16**:9274–9281 (2000).
54. D. R. Ulrich. Chemical Processing of Ceramics. *Chemical & Engineering News.* January 1: (1990).
55. W. B. Russel, D. A. Saville, and W. R. Schowalter. *Colloidal Dispersions*. Cambridge University Press, Cambridge, 1999.
56. I. Gonda. Development of a systematic theory of suspension inhalation aerosols. I. A framework to study the effects of aggregation on the aerodynamic behavior of drug particles. *Int. J. Pharm.* **27**:99–116 (1985).
57. J. D. Engstrom, D. T. Simpson, E. S. Lai, R. O. Williams III, and K. P. Johnston. Morphology of protein particles produced by spray freezing of concentrated solutions. *Eur. J. Pharm. Biopharm.* **65**:149–162 (2007).
58. Y.-F. Maa, P.-A. Nguyen, K. Sit, and C. C. Hsu. Spray-drying performance of a bench-top spray dryer for protein aerosol powder preparation. *Biotechnol. Bioeng.* **60**:301–309 (1998).
59. M. Gordon, and J. S. Taylor. Ideal copolymers and the second-order transitions of synthetic rubbers. I. Noncrystalline copolymers. *J. Appl. Chem.* **2**:493–500 (1952).
60. J. Hu, K. P. Johnston, and R. O. Williams III. Stable amorphous danazol nanostructured powders with rapid dissolutions rates produced by spray freezing into liquid. *Drug Dev. Ind. Pharm.* **30**:695–704 (2004).